VR based strabismus diagnosis using image processing (Conference Presentation)

Conference Paper · March 2019

DOI: 10.1117/12.2514254

4 authors, including:

Hweekwon Jung
Chonnam National University
19 PUBLICATIONS **20** CITATIONS

SEE PROFILE

Gyuhae Park
Chonnam National University
167 PUBLICATIONS **4,531** CITATIONS

SEE PROFILE

Hwan Heo
Chonnam National University
85 PUBLICATIONS **582** CITATIONS

SEE PROFILE

Virtual reality-based measurement of ocular deviation in strabismus

Yinan Miao[a], Jun Young Jeon[a], Gyuhae Park[a], Sang Woo Park[b], Hwan Heo[b,*]

[a] Department of Mechanical Engineering, Chonnam National University, Gwangju, 61186, South Korean
[b] Department of Ophthalmology, Chonnam National University Medical School and Hospital, 42, Jebong-ro, Dong-gu, Gwangju, 61469, South Korea

Abstract

Background and objective: Strabismus is an eye movement disorder in which shows the abnormal ocular deviation. Cover tests have mainly been used in the clinical diagnosis of strabismus for treatment. However, the whole process depends on the doctor's level of experience, which could be subjected to several factors. In this study, an automated technique for measurement of ocular deviation using a virtual reality (VR) device is developed.

Methods: A VR display system in which the screens that have the fixation target are changed alternately between on and off stages is used to simulate the normal strabismus diagnosis steps. Patients watch special-designed 3D scenes, and their eye motions are recorded by two infrared (IR) cameras. An image-processing-based pupil tracking technique is then applied to track their eye movement. After recording eye motion, two strategies for strabismus angle estimation are implemented: direct measurement and stepwise approximation. The direct measurement converts the eye movement to a strabismus angle after considering the eyeball diameter, while the stepwise approximation measures the ocular deviation through the feedback calibration process.

Results: Experiments are carried out with various strabismus patients. The results are compared to those of their doctors' measurement, which shows good agreement.

Conclusions: The results clearly indicate that these techniques could identify ocular deviation with high accuracy and efficiency. The proposed system can be applied in small space and has high tolerance for the unexpected head movements compared with other camera-based system.

Keyword: virtual reality, pupil tracking, computer vision, strabismus, cover tests.

1. Introduction

Strabismus is an eye movement disorder in which the eyes do not properly align with each other when looking at an object. For strabismus patients, only the healthy eye functions properly, while the misaligned eye, which is fixated in another direction, is not used to acquire an object image. The three main types of strabismus, esotropia, exotropia, and hypertropia can be distinguished based on the different directions of the ocular deviation [1]. This is a common eye disorder in which the vision of the deviated eye is constantly suppressed, resulting in amblyopia and even vision loss in children [2,3]. The psychosocial effect of strabismus includes negative impacts on self-imaging, interpersonal relationships, and working performance. Patients typically experience negative feelings from daily communication. In addition, the physical discomfort of the eye significantly affects the quality of their life, which can be considered as a disability [4, 5]. Various population-based studies have shown that many people suffer from this disease. The prevalence of strabismus is predicted to be near 5% in the general population older than six years old [6]. Like other ocular disorders, strabismus is usually treated with surgery that corrects the misalignment by adjusting the lengths of the extraocular muscles. Therefore, the accurate measurement of ocular deviation angle in strabismus is crucial for the treatment surgery.

Prism cover test (PCT) and Hirschberg test (HT) are the two primary tests used for clinical measurements, in which the former requires patient cooperation to continue fixating on a target, while the latter measures the ocular deviation angle based on the relative position between the light reflex and the pupil center. The HT is only used when patients are uncooperative or show poor fixation [7]. The PCT has been shown to be the most accurate, but it is still affected by subjective factors, such as the eye movement evaluation, the experience level of the doctor, and the cooperation of the patient, leading to different results when examined by different specialists, even when they are well trained [8].

The diagnosis of strabismus using a computer has been a popular research topic, and eye tracking has been used as an effective tool for this purpose [9]. The crucial point

* Corresponding author
E-mail address: youngnaiveman@gmail.com (Yinan Miao) , pokerface9811@gmail.com (Jun Young Jeon), gpark@chonnam.ac.kr (Gyuhae Park), exo70@naver.com (Sang Woo Park), Intereye@empal.com (Hwan Heo).

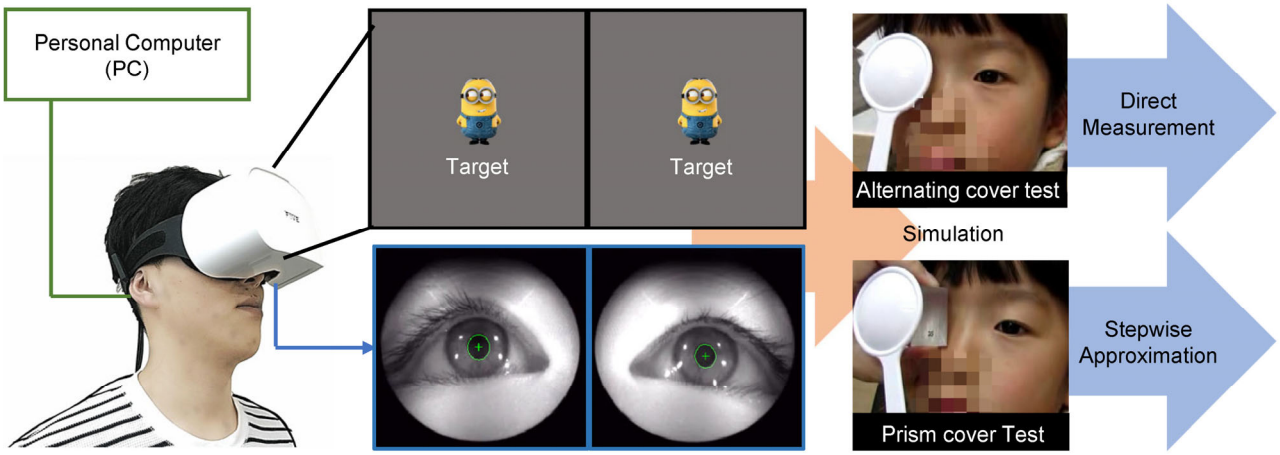

Fig. 1. Proposed VR-based strabismus diagnosis system with two proposed measuring techniques. The system, composed of a PC and a VR headset, can simulate the real strabismus examination environment. The target is a 'Minions' character right in front of the patient at a 6 m distance.

of such diagnosis is correctly identifying the eye position and/or the gazing direction from which the strabismus information can be extracted. Chen et al. [10] achieved the automated strabismus detection using convolutional neural networks. Chen et al. [11] used a consumer-grade eye tracker to acquire gaze data for strabismus diagnosis, which could provide the presence, type, and severity of strabismus but without specific deviation angles. Bakker et al. [12] developed an accurate eye tracking system for quantifying strabismus, which was capable of providing the gaze direction with an accuracy of 0.5°. The validation experiment was carried among only orthotropic adults. The performance under the real clinic environment is currently underway. The techniques presented in [13-15] could extract the light spot and the iris center for automated HT. However, HT requires the Hirschberg ratio and angle Kappa that are subject-independent, which significantly affects the accuracy.

Techniques based on the alternating cover test (ACT) are proposed in [16-18], where the ocular deviation angle is generated from the eye movement while alternating the cover. Chin rest must be used for resisting the relative position change between a patient and a target throughout the experiment, however, small errors are avoidable. The target distance adjustment, occluder moving, and real time measurements also imposes difficulties to these ACT-based techniques.

Thus, improving the accuracy, efficiency, and operating convenience are still necessary for these techniques to be implemented into practical applications.

Over the past few decades, virtual reality (VR) has significantly evolved for both personal and professional uses, and the cost is no longer a challenging parameter for practical applications [19]. VR can create impressive 3D scenes using a common personal computer (PC), making it possible to simulate the standard strabismus examination.

In this work, a VR-based real-time system for the measurement of ocular deviation using pupil tracking is proposed. The system can be set up with a common PC and a low-cost VR headset, which allows applications in a small space and has a high tolerance for the unexpected head movements compared to other camera-based systems.

Two unique diagnosis techniques, direct measurement (DM) and stepwise approximation (SA), are developed based on the ACT and the PCT, respectively. DM overcome the limitations of the current ACT-based techniques. SA simulates the golden standard, PCT, providing more accurate results than the ACT-based techniques.

The running time of each technique for measurement is less than 1 minute. The results are displayed immediately after the measurement through a MATLAB GUI interface developed for this study. The results are also compared to a doctor's diagnostic results in order to validate the accuracy of the proposed system.

2. VR-based ocular deviation measurement system

2.1. Methodology

The proposed system with a VR device and pupil tracking could replace the diagnostic procedure of a doctor using cover tests. During the PCT, patients should be seated and asked to fixate on an accommodative target at a fixed distance, while the doctor should alternate an occluder between eyes and observe the eye movement. Thus, the three key points of cover tests are the target, the occluder, and the eye movement evaluation, which can be easily simulated, as shown in Fig. 1. A detailed description is given below:

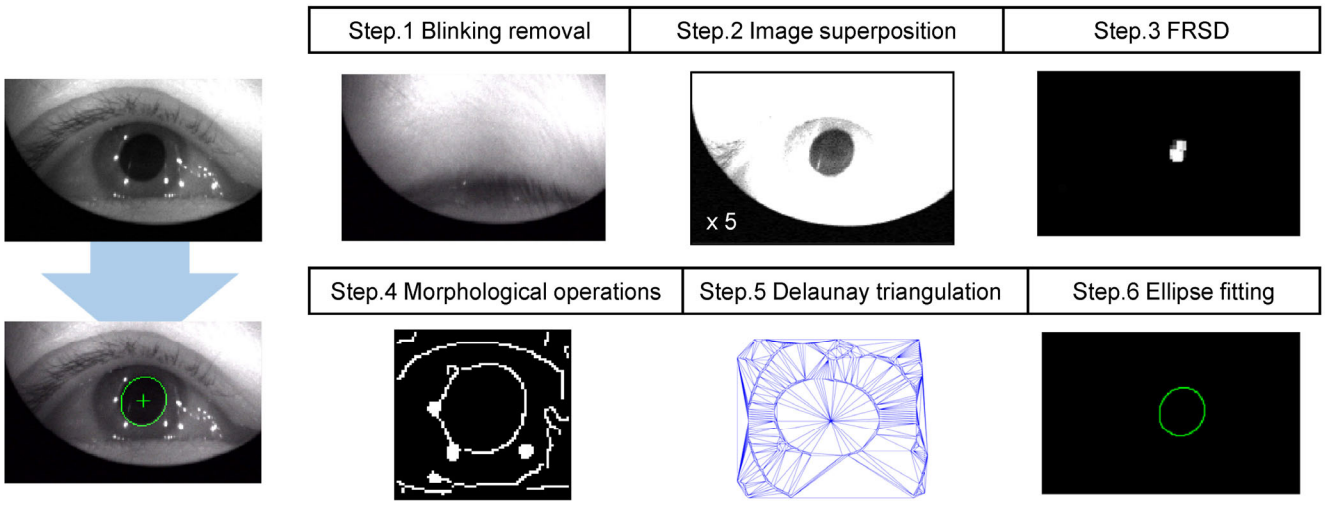

Fig. 2. Process of pupil tracking: 1) the blinking image is removed based on the blinking feature V_B; 2) image superposition is applied to create an image with a clear pupil; 3) FRSD is used for the acquired image to roughly locate the position of the pupil; 4) an edge image is extracted; 5) the edge line of pupil is caught by Delaunay triangulation; 6) the clear pupil boundary is acquired as an ellipse close to the real shape.

1) *Target*
   The target is displayed inside a VR headset with a pre-designed scene. The properties that can be controlled using this technique include the size, position, and shape. In order to get the patient's attention, especially when the patient is a child, various targets are used during the test.
2) *Occluder*
   The occluder is used to temporarily block the light to one eye, which can be simulated by controlling off and on states of the display screen in front of each eye, which strictly follows the standard measuring rule.
3) *Eye movement evaluation*
   Eye movement is tracked in real-time using the pupil tracking technique under infrared (IR) light. The motion of a pupil center is recorded and used for further analysis.

Based on this system mentioned above, two automated diagnosing techniques are developed in this study: direct measurement and stepwise approximation. DM simulates the occluder switching of the ACT by controlling the screen. A 'jump' of the eye can be observed on strabismus patients and then quantified using the proposed technique. SA simulates the PCT. In the same way that a prism creates a virtual target in the eye over which it is placed, SA displays two different targets on two screens in order to have the same effect as a prism. The position of the 'virtual target' is converted to a strabismus angle after reaching the proper position that leads to no eye movement when alternating the cover.

2.2. System description

The diagnosis system used in this study is composed of two common devices: a VR headset and a personal computer. The VR device used is an eye tracking headset equipped with an IR camera system. Six powerful IR lights provide illumination for tracking eye movements. In our study, a VR device, a FOVE [20], is used. The screen is WQHD OLED with a resolution of 2560x1440 which can work at 70 frames per second (fps). The headset is connected to a PC through two USB 3.0 and one HDMI cables. MATLAB [21] and Unity 3D [22] are used to run the tracking codes and control the VR. A MATLAB GUI with all functions is created for operating convenience.

Prior to examination, patients are asked to wear the VR headset and fix it tightly on their head. In the VR device, they can see a square space with one target. Patient's sight in VR is restricted to only watch forward in order to sustain the relative position of the target and the patient. Throughout the test, patients are only requested to fixate on the target.

Pupil tracking technique is considered as one of the most important tools in this study, which could measure the eye reaction under different processes. The related work of pupil tracking is shown in the subsection 2.3. The pupil tracking technique is illustrated in the subsection 2.4. The theories and procedures of the two techniques (DM and SA) are discussed in detail in sections 3 and 4. The experimental results of both techniques are presented in section 5.

2.3. Related work on pupil tracking

In this study, the pupil is assumed as the center of the eyeball that represents the starting point of the gaze direction for most people. The most important characteristic of the pupil is that it shows an obvious difference from other tissues of an eye under IR light,

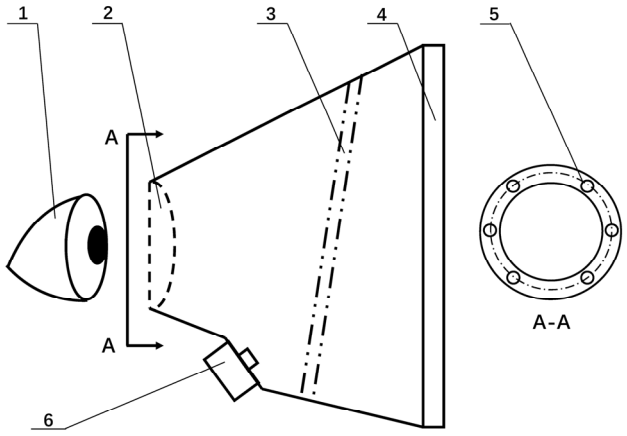

Fig. 3. IR camera system in FOVE headset. 1) User's eye. 2) VR lens. 3) Hot mirror that only reflects IR light. 4) Screen. 5) IR LEDs. 6) IR camera.

resulting in more robust tracking.

Wu and Lee et al. [23, 24] proposed the pupil recognition techniques using deep learning, which could measure the rough pupil position. The binary image of pupil produced by threshold-based image segmentation has been commonly used in pupil tracking. Swirski and Javadi et al. [25, 26] developed the pupil tracking techniques that operates on the pupil binary image to extract the pupil outline. Thus, a high contrast pupil image captured under sufficient IR light is required to accurately estimate the position of pupil.

Operation on the edge image of pupil after applying the edge detecting filters is another tool to for accurate pupil detecting. Fuhl et al. [27] did both morphologic and algorithmic approaches to locate the edge line that represents the pupil. Li et al. [28] applied the pupil deformation model and the eye model to the pupil tracking techniques to extract the right pupil from edge images. These techniques show excellent detection rate on processing the pupil images taken in the wild environment, which, however, needs much calculation on removing the effects from the noise in wild environments.

2.4. Pupil tracking algorithm

The diagram of the IR camera system in FOVE [20] is shown in Fig. 3. This system contains lens, IR camera, IR LEDs, hot mirror, and screen. A hot mirror that only reflects IR light is mounted between the screen and the human eyes, enabling the camera to capture the good front view of user's eyes. Six IR LEDs are distributed around the lens (see 5 in Fig.3). However, the near LEDs could not provide enough illumination due to the small space in headset, resulting in a low-contrast and dark pupil image.

The approach [29] is adopted because of the low computation cost and the powerful tracking ability. The pupil tracking algorithm consists of four steps: Fast Radial Symmetry Detector (FRSD), Morphological operations, Delaunay Triangulation, and Ellipse fitting (see steps 3-6 in Fig. 2). First, FRSD is applied on an acquired image in order to roughly locate the position of a pupil, which is normally a circular area. In the second step, an edge image is extracted by a canny edge operator with a morphological operation to remove glints and useless edges. Third, the pupil outline is captured through Delaunay triangulation by adding a point which is used to estimate the pupil center. Finally, using ellipse fitting, the pupil boundary is acquired as an ellipse close to the real shape with certain parameters. The center of the pupil, which is related to the gaze direction, is returned for the subsequent data analysis. A detailed description of this process is shown in reference [29].

The low performance under low-illuminated case is overcome by applying the image superposition (see steps 2 in Fig. 2). Blink removal (see steps 1 in Fig. 2) also helps to reduce the portion of meaningless data, which is crucial for the measurement in 3 seconds (time interval of alternating cover) because one blinking may take 0.3 - 0.4 seconds.

During the measurement, eye blinking during the pupil tracking may lead to significant estimation errors. In order to remove eye blinking, a feature that represents the difference between the current frame and the open-eye sample is used to identify cases of blinking as

$$V_B = \sum_{x=0}^{w-1} \sum_{y=0}^{h-1} (\left| I_{cf}(x,y) - I_{os}(x,y) \right|) \quad (1)$$

where, V_B is a blinking feature value that represents the sum of the intensity of all pixels, h is the height of an image in pixel, w is the width of an image in pixel, I_{cf} is the intensity image array of the current frame, and I_{os} is the intensity image array of an open sample.

The V_B increases significantly when people close their eyes, and this can be recognized and removed from further analysis. The threshold of blinking is selected as 10 times the image size (200000, for the used image size, 100*200 in pixels) of the increasing value of V_B between two frames which could not be reached by simply rotating eyes.

In practice, the tracking process may also be affected by the different face and eye characteristics of different patients. For example, patients with small eyes or a flat face cannot be completely lightened while wearing a VR headset, resulting in a video without a clear pupil captured. Therefore, image superposition is used to reduce these kinds of negative effects of dark lighting condition as

$$I_{is}(x,y) = \begin{cases} I_{ori}(x,y) * \alpha & for\ I_{ori}(x,y) * \alpha < 255 \\ 255 & for\ I_{ori}(x,y) * \alpha \geq 255 \end{cases} \quad (2)$$

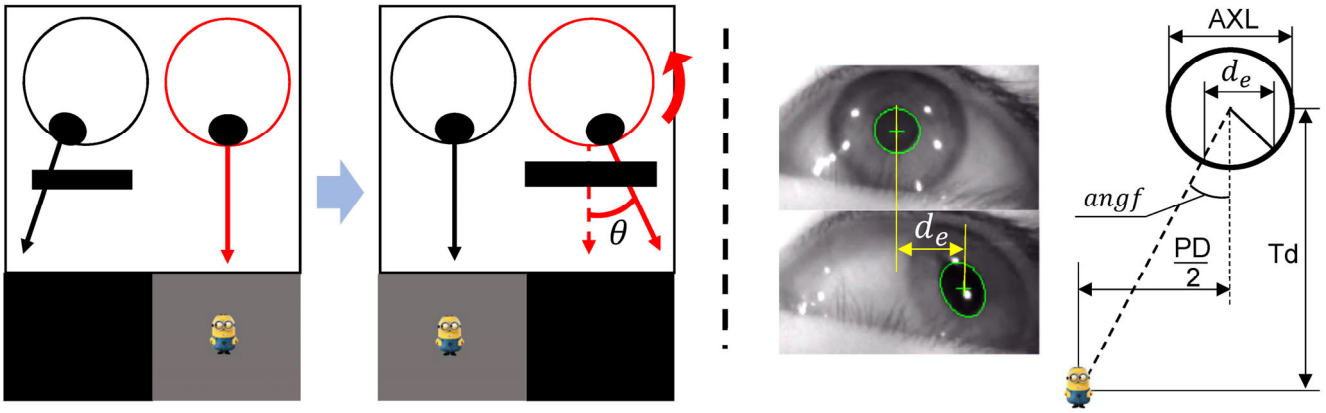

Fig. 4. Left part: ACT is described by two states, covering the healthy eye (black) and covering the misaligned eye (red). A 'jump' can be observed while alternating cover. VR screen is shown in the bottom of the image to demonstrate how it simulate the occluder and target. Right part: the 'jump' is quantified using pupil tracking using our system. The convergence angle of eye, $angf$, caused by fixation is shown in the schematic drawing in which the eye is assumed to look at a near target (0.1 m ahead from the eye) resulting in a large convergence angle.

where, I_{is} is the resulting intensity image array under a certain scale factor, I_{ori} is the intensity image array of the original image, and α is the scale factor of which the default value is 5.

Under IR light, pupils are known to be the darkest part against other tissue. With values of α that are larger than 1, the intensity difference between the dark part (the pupil) and the bright part (the other parts of eye) will be increased by the factor of α, which results in a more ideal image for FRSD that calculates based on the intensity difference to locate the pupil.

3. Direct measurement

The ACT is one of the cover tests used to determine the presence of strabismus. When the normal eye is covered, the misaligned eye fixates on the target in front of it whereas the normal eye deviates from the primary position, as illustrated in Fig. 4. After alternating the occluder, the eye rotates back to focus on the target for image alignment. At the same time, the misaligned eye behind the occluder rotates with the same degree, which indicates the deviation. Different directions of this deviation lead to different types of strabismus. However, a doctor cannot quantify the observed movement (see the right part of Fig. 4) using their naked eyes.

3.1. Direct measurement

DM is a method that can automatically measure the angle θ by simulating the real ACT. It combines a VR device and the eye tracking technique described in the previous section. The target and the function of occluder are simulated inside a VR device, while the eye movement is captured and processed for automated diagnosis. Typically, multiple measurements (at least three) are taken and averaged in order to improve the accuracy.

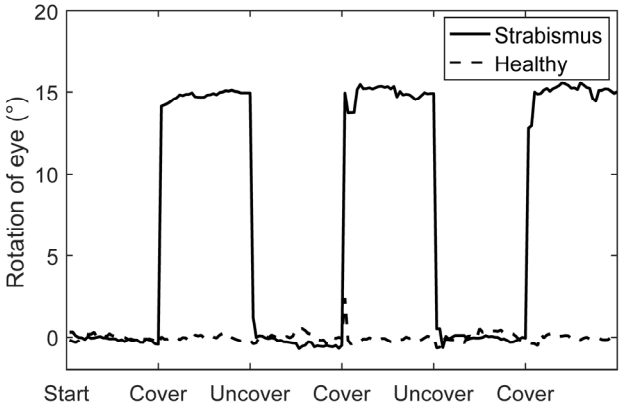

Fig. 5. Comparison between healthy people and strabismus patients using DM. Three 'jumps' occurred right after covering the misaligned for strabismus patient. On the contrary, healthy people remain stable around zero degree from start to the end.

The detailed steps to simulate the ACT is described below:

1) *Close the screen in front of the healthy eye and open the other one*
   Identical to the doctors' process, the healthy eye cannot see anything except darkness, so the misaligned eye is used to fixate on the target. This state is sustained for three seconds to track the misaligned eye. The current position is recorded and set as an initial position.
2) *Open the screen in front of the healthy eye and close the other one*
   The misaligned eye deviates from the initial position. The deviated eye position is recorded for three seconds from which the ocular deviation angle is estimated.
3) *Repeat steps 1) and 2) two times*
   The results of the three measurements are averaged to improve the accuracy.
4) *Estimate the ocular deviation angle*
   The ocular deviation angle is estimated by converting eye movements to the rotation of an eyeball.

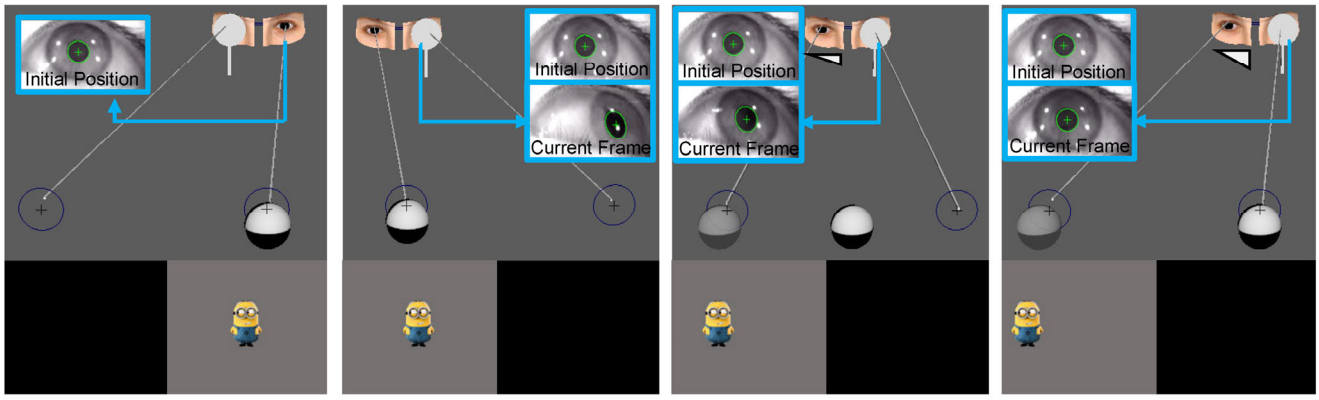

Fig. 6. Four states of stepwise approximation (the bottom part shows the occluder and target simulation of the top part in VR): a) the initial position of the misaligned eye (the left eye of the model) is recorded and set as zero while the healthy eye is covered; b) the misaligned eye deviates from initial position after alternating the cover; c) the virtual image created by the prism (white triangulation with black outline) presents at another position as simulated in VR by changing the position of the target(Minions), so the misaligned eye comes near the initial position; d) the virtual image reaches the proper position by increasing the prism diopter, making the misaligned eye return to the initial position. The ocular deviation angle is estimated from the virtual image position and the target distance.

The tracking result of an intermittent exotropia patient with 15° is shown in Fig. 5. The signal from the patient deviates from zero and remains stable at a certain value which represents the deviation angle. By contrast, healthy people present a real-time signal that remains stable around zero from the start to the end.

3.2. Deviation angle estimation

The rotation of the misaligned eye is represented by the position change of the pupil center on the captured two-dimensional image. It is recorded by pupil tracking and converted to angle θ, as given by

$$\theta = arcsin\left(\frac{d_e * mp - 0.5 * AXL * sin(angf)}{0.5 * AXL}\right) + angf \quad (3)$$

Where, d_e is the deviated distance of eye in pixels, mp is the convert rate from pixel to mm, PD is the pupillary distance, AXL is the axle length measured by a professional machine, Td is the distance between the target and the eye, and $angf = arctan(PD/2 * Td)$, is the convergence angle as described in the right part of Fig. 4.

In this equation, the eyeball is assumed to be a ball of which the axle length is the diameter. Thus, the rotating angle can be calculated from the position change of the pupil center. The pupillary distance (PD) is considered for two eyes that cannot completely look forward. A fixed angle exists between two eyes that is related to PD. A farther distance of the target leads to a smaller degree of this convergence angle.

4. Stepwise approximation

In contrast to the ACT, the PCT measures the ocular deviation angle by eliminating the "jump" while alternating the occluder using a prism. This feature is also used as a base of SA. During the PCT, patients are instructed to look at a target by a doctor. The prism is used to create a virtual image of a target at another position according to the prism position and diopter. For the patient, two targets can be seen: a real target while using one (misaligned) eye and a virtual target while using the other eye. The virtual target can be moved by changing the prism diopter. Once the virtual target is moved to the right position, the misaligned eye should fixate on the real target while the normal eye focuses on the virtual target, which indicates that there is no eye movement while the doctor alternates the occluder. The ocular deviation angle is quantified by checking the amount of prism power in the prism diopter (Δ). The rate of transferring it to degrees (°) is normally set as 1.75/1 (Δ/°).

4.1. Stepwise approximation

Compared to DM, SA adds the function of the prism, as demonstrated in Fig. 6. Both the 'real target' and the 'virtual target' are separately simulated on two screens. The steps of SA are illustrated as below:

1) *Close the screen of the healthy eye and open the other one*
   The initial position of the misaligned eye is acquired while it fixates on the 'real target'.
2) *Open the screen of the healthy eye and close the other one*
   The tracking result of the current frame shows a clear difference compared to the initial position (see in Fig. 6a).
3) *Move 'virtual target'*
   The 'virtual target' (see the transparent ball in Fig. 6c) is moved according to the difference obtained in step 2). The difference is then updated after tracking the current frame.

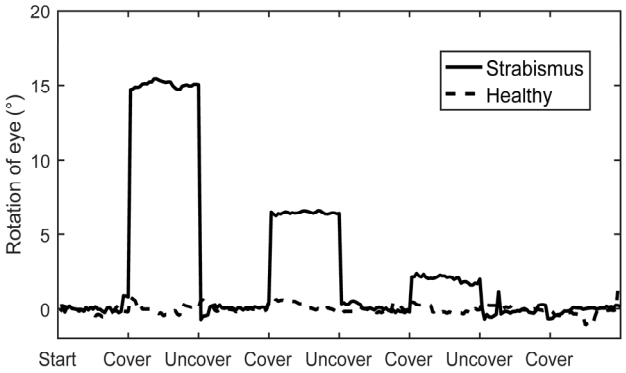

Fig. 7. Comparison between healthy people and strabismus patients using SA. Rotation of eye (°) versus covering state. Tracking result of patient approaching zero step-by-step as the feedback process proceeds while the healthy people remained stable on zero.

4) *Repeat step 3) until difference reaches zero*
   When the 'virtual target' reaches the proper position, the difference between the current frame and the initial position should be zero, which ends the iterative process.
5) *Estimate the ocular deviation angle*
   The strabismus angle is then quantified based on the position of the 'virtual image'.

Fig. 7 shows the changes in pupil center position throughout the process. The angle of the deviated eye gradually approaches zero as the feedback process progresses, while the eyes of healthy people remain stable at zero.

4.2. Deviation angle estimation

The strabismus angle, θ, can be estimated from the distance between the 'virtual image' and the 'real image'. The following equation is used:

$$\theta = arctan\left(\frac{2*d_t - PD}{2*Td}\right) + arctan\left(\frac{PD}{2*Td}\right) \quad (4)$$

where d_t is the target moving distance in virtual environment, PD is the pupillary distance, and Td is the distance between the target and the eye.

As shown in (4), no axle length is required. Compared to DA, SA does not require information on the eyeball diameter to estimate the strabismus angle, which could reduce the estimation error. The calibration process improves the diagnosis accuracy and avoids some occasional cases that may happen in the open-loop process.

5. Experiment

5.1. Setup

The proposed system is set up inside the Chonnam National University Hospital. In total, seventeen patients

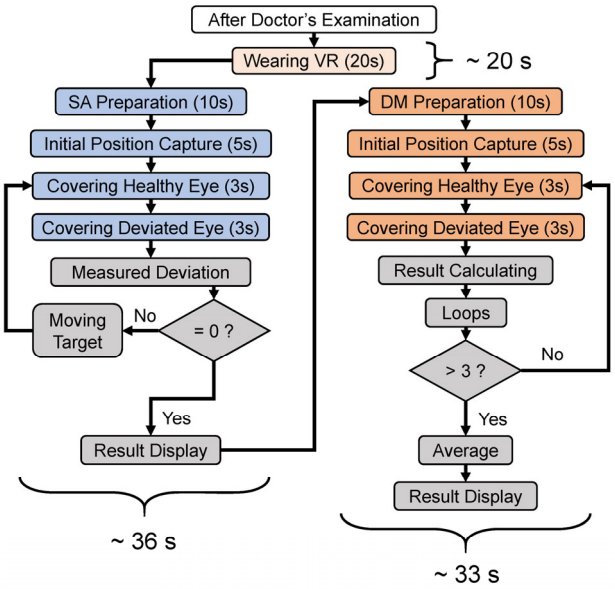

Fig. 8. Flow chart of the experiment. The time of each step is attached in brackets. The process in the gray blocks could be finished within several milliseconds.

over six years old are examined using the proposed strabismus diagnosis system, including five orthotropia and twelve exotropia. They all have low myopia < 2 Δ. Patients with poor cooperation or other eye diseases are excluded from the analysis. Informed consent was obtained from all 17 people who were eligible and ultimately enrolled in this experiment. The experimental protocol adhered to the guidelines of the Declaration of Helsinki.

The detailed experimental process is shown in Fig. 8. Prior to a test, each patient is diagnosed by a doctor. The PCT is conducted by a doctor at a distance fixation using a 'Minions' toy at six meters. Then, SA and DM are carried out within thirty minutes of the doctor's diagnosis. The total measurement time ranged from 1.5 to 2 minutes depending on the patient. Throughout the experiment, only one operator without having any knowledge on strabismus is required to operate on the GUI.

In the experiment, the patients are required to wear the VR headset tightly and focus on the target image. Ten images of different 'Minions' characters switching at a three-second interval are set as the target to attract the patient's attention. The size is 15cm x 20 cm in VR. The target distance inside the VR is set as 6 m, which is identical to that of the doctor's real fixation test. In addition, the pupillary distance and the eyeball diameter are provided by the doctor.

5.2. Comparison of VR and real world

The VR users appear to have misperception on space and motion. Two important factors and their effects on the distance perception are discussed in this section.

Table 1
Diagnostic result (°) of doctor, DM, and SA.

Result	Doctor	SA	DM	Result	Doctor	SA	DM	Result	Doctor	SA	DM
Patient 1	0	1.3	5.1	Patient 7	2.3	0.3	1.4	Patient 13	10.3	5.8	5.9
Patient 2	0	0.6	0.7	Patient 8	3.4	1	2.6	Patient 14	11.4	11.6	10.9
Patient 3	0	0.5	0.3	Patient 9	6.9	5.9	6.0	Patient 15	14.3	13.4	12.6
Patient 4	0	0.4	0.6	Patient 10	8.6	8.0	8.4	Patient 16	17.1	13.8	13.6
Patient 5	0	0.1	0.3	Patient 11	10.3	12.8	11.5	Patient 17	17.1	15.3	15.2
Patient 6	2.3	2.4	2.1	Patient 12	10.3	10.4	9.9				

The first factor is the mismatch between PD of patients and PD of VR headset. The FOVE has the fixed PD with a value of 63.5 mm which is related to the commonest value for human vision. The target is perceived at a farther distance for the patients with small PD and becomes closer for the patients with large PD.

The second factor is distance compression in the virtual environment. Recent research has observed the distance underestimation with the consumer-grade VR headset. Peer et al. [30] measured the individual's distance compression with a 20% relative percent error (RPE) of average underestimation, in which RPE indicates the difference of the perceived distance measurement between a real environment and a virtual environment.

Those effects from two factors on the proposed system at a measuring distance of 6 m is discussed here. For example, a 20% distance compression make the target to be perceived at 4.8 m (6 m * 0.8) which would cause an eye rotation as in equation (5):

$$E_r = arctan(\frac{PD_u}{(1-RPE)*Td}) - arctan(\frac{PD_u}{Td}) \quad (5)$$

where, E_r is the deviation error caused by distance compression, PD_h is the PD of users, RPE is relative percent error, and Td is the target distance in FOVE.

A 20 % RPE (Td, 6 m; PD, 63.5 mm) would only cause an error degree about 0.15°, which complies with a common sense that the light from a far target entering the human eye is considered near-parallel. A 15 mm mismatch of PD (Td, 4 m; RPE, 0%) would cause an error degree about 0.14°. Though these errors are not so significant at the measuring distance of 6 m, some correcting procedures are implemented for each patient before starting a test. The background, which is a wall in VR, is set at the same distance as the target to reduce the effect of distance compression, and also no other objects are displayed except the wall and target. The rendering PD in Unity 3d (the distance between rendering cameras of the left eye and the right eye) is adjusted to be the same as the patient's PD. The center line of headset is roughly matched with the center line of two eyes using the preview of IR camera.

Table 2
Mean deviations of ocular deviation angle excluding error cases.

Mean Deviation (°)	Orthotropia	Exotropia	Total	Difference
Doctor	0.0 ± 0.0	8.7 ± 5.0	6.2 ± 5.8	/
SA	0.5 ± 0.2	8.0 ± 4.8	5.9 ± 5.4	0.3 ± 0.9
DM	0.4 ± 0.2	8.1 ± 5.5	5.9 ± 5.8	0.3 ± 1.3

However, the errors could be magnified once the system measures strabismus at the distance of 0.33 m, which is also an important step of strabismus measurement. Correcting the distance estimation through either rendering manipulation or addition of sensory information are currently being developed.

5.3. Results

Three results acquired for each patient from the doctor, DM, and SA experiments are used to evaluate the performance of the proposed technique. As shown in Table 1, both of the techniques were consistent with the doctor's results.

The mean deviations (mean ± standard deviation) of all of the examinations (see in Table 2) are calculated in order to give a clear comparison excluding patients 1, 13, and 16 which show noticeable differences (3.3°-5.5°) from the doctor's results.

For the first patient, the movement of the headset relative to his head was observed, which distorted the initial position as shown in Fig. 9. Throughout the examination, the relative position between the headset and the patient keeps changing, which significantly increase the eye deviation. For patients 13 and 16, the doctor diagnosed them with having a poor fixation on the target. For those patients could not sustain the fixation on the target, a doctor cannot diagnose a 100-percent correct deviation. As shown in Fig. 10, the patient 13 could not completely focus on the target. When the eyes aim the target, the exact position remains uncertain.

The total results of the two techniques were 5.9° ± 5.8° and 5.9° ± 5.4° compared to 6.2° ± 5.8°, showing exactly

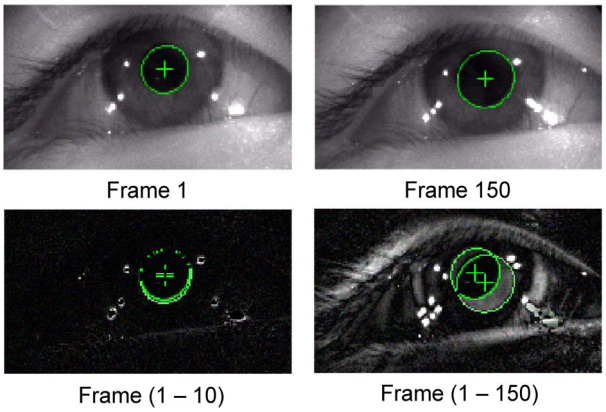

Fig. 9. The eye initial position change caused by the headset moving on patient 1. The lower part shows the difference between two frames.

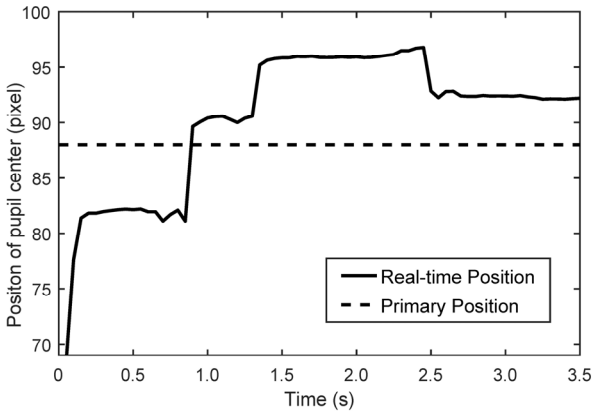

Fig. 10. Horizontal pupil position when the patient 13 focused on one fixed target. The roughly estimated primary position of the patient is plotted in the dashed line.

similar distributions. The 10 exotropia patients were 8.1° ± 5.5° and 8.0° ± 4.8° compared to 8.7° ± 5.0°, and the four orthotropia patients were 0.4° ± 0.2° and 0.5° ± 0.2° compared to 0° ± 0°.

The mean difference between the two techniques and the doctor's results for all of the patients were all less than 0.7°. This value is insignificant enough because the degree of 1.15° is normally the threshold of observing an eye movement under optimal circumstances [31]. A smaller rotation of the eyes than that cannot be recognized by naked eyes.

Inter-examiner reliability of the measurement has been an important topic for strabismus examinations; this is because many factors may influence the results in the PCT with different examiners, such as fixating points on the target, position of the examiner, and the rotation of prism [32]. Hrynchak and Holmes et al. [32, 33] showed that the difference less than 2.85° (5 Δ) is well within test-retest variability. The 95% limits of agreement (1.96 x standard deviation of the difference) in our experiment between the doc and DM and between the doctor and SA are ±2.5° and ±1.76°, respectively. They are all less than 2.85°, indicating the accuracy of our technique.

Both DM and SA show excellent performance on the measurement of a deviation angle in orthotropia and exotropia. It could be stated that SA produces more stable results than DM on the 95% limit of agreement of difference. DM requires the accurate axle length of a patient, which should be measured by other inspection machines, in order to calculate the deviation angle. In cases in which the hospital is not equipped with that machine or the axle length is not measured accurately, SA should be considered as the better tool, because it contains feedback calibrating process to estimate the angle, such as the real PCT.

It could also be stated that, compared to the PCT carried out by a doctor, DM and SA reduce errors caused by several subjective parameters. Specifically, in our system, the relative position of the target to a patient, and of a patient to an examiner, remain the same, whereas all those relative positions may change even under the inspection of experienced doctors in the PCT. In addition, the environment in VR is simplified, which reduces the effect of other objects. The target is designed to be more interesting in a VR device in order to attract the attention of a patient. Pupil tracking is applied for more objective and accurate observation of eye motion instead of using naked eyes, which is also capable of tracking smaller movements.

5.4. Discussion and future works

In this subsection, the error sources in the proposed strabismus diagnosis system and the future works are discussed in detail.

1) *Moving of headset*

In our system, the relative positions of the head and the VR headset should be maintained from the start to the end. These influence the initial position, which is the first step of estimating the difference. Patients are asked to fix the headset tightly on their head. However, in some cases (such as young children), the headset is too big, which produces estimation errors; therefore, more cushion or an adjustable headset could be used to reduce the effect of moving of the headset.

2) *Pupil tracking*

One of the important parts of the proposed system is pupil tracking, which provides the bases of all the calculations. Even though we already had robust results for most of the patients, in some cases, including eyes that were too small or lush eyelashes that covered the pupil, the pupil center could not be accurately tracked. More robust algorithms under various cases should thus be considered.

3) *Vertical strabismus*

The vertical strabismus is not tested in this work because of a lack of available patients. However, this

proposed system is capable of diagnosing those types of strabismus using the same procedure. Unlike measurements for horizontal strabismus, the pupils of hypertropia and hypotropia patients are usually blocked by an eyelid, so only half the pupil is captured by a camera; tracking only half the pupil may not be accurate for DM. However, SA measures the strabismus angle by comparing the initial position and the final position, in which the pupil is always looking forward. It could serve as an effective tool for evaluating vertical strabismus.

4) *Near test at 0.33 m or flexible measuring distances*

Our system mainly focuses on the far test at 6 m, which already shows good performance. However, flexible measuring distances, including near test at 0.33 m, are required in strabismus diagnosis. This will be another important topic that will be investigated in the near future.

6. Conclusion

In this work, we developed a VR-based real-time system for measurement of ocular deviation angle which can be easily used with a common personal computer and a VR headset for applications in small space and with a high tolerance for the unexpected head movements compared with other camera-based systems. Two techniques are developed based on this system to accurately assess the deviation angle in strabismus: direct measurement and stepwise approximation.

In this system, we applied an advanced pupil tracking technique to acquire the eye motion. The direct measurement directly estimates the strabismus angle based on the motion of the eye. The stepwise technique uses real-time feedback to estimate the strabismus angle. Patient tests are carried out with both techniques, and the results are compared with the doctor's measurement result. The results show that the proposed technique could accurately and efficiently assess the ocular deviation angle.

Conflict of interest

We declare that we have no financial or non-financial conflicts of interest to disclose.

Acknowledgment

This research was supported by Basic Science Research Program through the National Research Foundation of Korea (NRF) funded by the Ministry of Education (NRF-2017R1D1A3B03032579)

References

[1]K.W. Wright et al., *Pediatric ophthalmology and strabismus,* 2nd ed. New York, NY, USA: Springer-Verlag, 2013, pp. 84–102.

[2]S.A. Cotter et al., "Risk factors associated with childhood strabismus: the multi-ethnic pediatric eye disease and Baltimore pediatric eye disease studies," Ophthalmology, vol. 118, no. 11, pp. 2251-2261, Nov. 2011. https://doi.org/10.1016/j.ophtha.2011.06.032.

[3]T. Torp-Pedersen et al., "Perinatal risk factors for strabismus," International journal of epidemiology, vol. 39, no. 5, pp. 1229-1239, Oct. 2010. https://doi.org/10.1093/ije/dyq092.

[4]S.E. Olitsky et al., "The negative psychosocial impact of strabismus in adults," Journal of American Association for Pediatric Ophthalmology and Strabismus, vol. 3, no. 4, pp. 209-211, Aug. 1999. https://doi.org/10.1016/S1091-8531(99)70004-2.

[5]S.R. Hatt et al., "The effects of strabismus on quality of life in adults," American journal of ophthalmology, vol. 144, no. 5, pp. 643-647, Nov. 2007. https://doi.org/10.1016/j.ajo.2007.06.032.

[6]D. Stidwill, "Epidemiology of strabismus," Ophthalmic and Physiological Optics, vol. 17, no. 6, pp. 536-539, Nov. 1997. https://doi.org/10.1046/j.1475-1313.1997.97000379.x.

[7]A.L. Rosenbaum, and A.P. Santiago, Clinical strabismus management: principles and surgical techniques. Philadelphia, PA, USA: W.B. Saunders Company, 1999, pp. 3–21.

[8]B.B. Rainey et al., "Reliability of and comparisons among three variations of the alternating cover test," Ophthalmic and Physiological Optics, vol. 18, no. 5, pp. 430-437, Sep. 1998. https://doi.org/10.1046/j.1475-1313.1998.00375.x.

[9]A.T. Duchowski, "A breadth-first survey of eye-tracking applications," Behavior Research Methods, Instruments, & Computers, vol. 34, no. 4, pp. 455-470, Nov. 2002. https://doi.org/10.3758/BF03195475.

[10]Z. Chen, "Strabismus recognition using eye-tracking data and convolutional neural networks," Journal of healthcare engineering, vol. 2018, April. 2018. https://doi.org/10.1155/2018/7692198

[11]Z. Chen et al., "Eye-tracking-aided digital system for strabismus diagnosis," Healthcare technology letters, vol. 5, no. 1, pp.1-6, Mar. 2018. https://doi.org/10.1049/htl.2016.0081.

[12]N.M. Bakker et al., "Accurate gaze direction measurements with free head movement for strabismus angle estimation," IEEE Transactions on Biomedical Engineering, vol. 60, no. 11, pp. 3028-

3035, Nov. 2013. https://doi.org/10.1109/TBME.2013.2246161
[13]J.D.S. De Almeida et al., "Computer-aided methodology for syndromic strabismus diagnosis," Journal of digital imaging, vol. 28, no. 4, pp. 462-473, Aug. 2015. https://doi.org/10.1007/s10278-014-9758-0.
[14]N. Khumdat et al., "Development of a computer system for strabismus screening" in BMEICON 2013, Amphur Muang, Krabi, Thailand, 2013, pp. 1-5. https://doi.org/10.1109/BMEiCon.2013.6687635
[15]D. Model, and M. Eizenman, "An automated Hirschberg test for infants," IEEE Transactions on Biomedical Engineering, vol. 58, no. 1, pp. 103-109, Jan. 2011. https://doi.org/10.1109/TBME.2010.2085000.
[16]T.L.A. Valente et al., "Automatic diagnosis of strabismus in digital videos through cover test," Computer methods and programs in biomedicine, vol. 140, pp. 295-305, March. 2017. https://doi.org/10.1016/j.cmpb.2017.01.002.
[17]M.W. Seo et al., "The Automated Diagnosis of Strabismus Using an Infrared Camera," in MBEC 2014, Dubrovnik, Croatia, 2015, pp. 142-145. https://doi.org/10.1007/978-3-319-11128-5_36
[18]Y. Zheng et al., "Intelligent Evaluation of Strabismus in Videos Based on an Automated Cover Test," Applied Science, vol. 9, no.4, pp. 731, Jan. 2019. https://doi.org/10.3390/app9040731.
[19]G. Riva, "Virtual reality for health care: the status of research," Cyberpsychology & Behavior, vol. 5, no. 3, pp. 219-225, Jun. 2002. https://doi.org/10.1089/109493102760147213.
[20]*FOVE 0*. (2017) [Online]. Available: https://www.getfove.com/
[21]*MATLAB*. (2016) [Online]. Available: https://www.mathworks.com/products/matlab.html
[22]*Unity*. (2019) [Online]. Available: https://unity.com/
[23]E.Q. Wu et al., "C Rotated Sphere Haar Wavelet and Deep Contractive Auto-Encoder Network With Fuzzy Gaussian SVM for Pilot's Pupil Center Detection," IEEE transactions on cybernetics, pp. 1–14, Jan. 2019. https://doi.org/10.1109/TCYB.2018.2886012
[24]Y.W. Lee et al., "Residual CNN-Based Ocular Recognition Based on Rough Pupil Detection in the Images by NIR Camera Sensor," Sensors, vol. 19, no. 4, pp. 842, Jan. 2019. https://doi.org/10.3390/s19040842
[25]L. Swirski et al., "Robust real-time pupil tracking in highly off-axis images," Proceedings of the Symposium on Eye Tracking Research and Applications, pp. 173-176, Mar. 2012. https://doi.org/10.1145/2168556.2168585
[26]A.H. Javadi et al., "SET: a pupil detection method using sinusoidal approximation," Frontiers in neuroengineering, vol. 8, pp. 4, Apr. 2015. https://doi.org/10.3389/fneng.2015.00004
[27]W. Fuhl et al., "Else: Ellipse selection for robust pupil detection in real-world environments," Proceedings of the Ninth Biennial ACM Symposium on Eye Tracking Research & Applications, vol. 2016, pp. 123-130, Mar. 2016. https://doi.org/10.1145/2857491.2857505
[28]J. Li et al., "A Geometry-Appearance-Based Pupil Detection Method for Near-Infrared Head-Mounted Cameras," IEEE Access, vol. 19, no. 6, pp. 23242-23252, Apr. 2018. https://doi.org/10.1109/ACCESS.2018.2828400
[29]N. Kumar et al., "A novel approach to video-based pupil tracking," in SMC, San Antonio, TX, USA, 2009, pp. 1255–1262. https://doi.org/10.1109/ICSMC.2009.5345909
[30]A. Peer and K. Ponto, "Evaluating perceived distance measures in room-scale spaces using consumer-grade head mounted displays," 2017 IEEE Symposium on 3D User Interfaces (3DUI), pp. 83-86, Mar. 2017. https://doi.org/10.1109/3DUI.2017.7893321
[31]E. Ludvigh, "Amount of eye movement objectively perceptible to the unaided eye," Am J Ophthalmol, 32, pp. 649, 1949.
[32]P.K. Hrynchak et al., "Comparison of alternate cover test reliability at near in non - strabismus between experienced and novice examiners," Ophthalmic and Physiological Optics, vol. 30, no. 3, pp. 304–309, May. 2010. https://doi.org/10.1111/j.1475-1313.2010.00723.x
[33]J.M. Holmes et al., "Defining real change in prism-cover test measurements," American journal of ophthalmology, vol. 145, no. 2, pp. 381-385, Fed, 2008. https://doi.org/10.1016/j.ajo.2007.09.012